Title

Amphibian yolk platelet ultrastructure visualized by freeze-etching

Journal

Journal of Ultrastructure Research, 40(1-2)

ISSN

0022-5320

Authors

Leonard, Robert
Deamer, David W
Armstrong, Peter

Publication Date

1972-07-01

DOI

10.1016/s0022-5320(72)80019-4

Peer reviewed

J. ULTRASTRUCTURE RESEARCH 40, 1–24 (1972)

Amphibian Yolk Platelet Ultrastructure Visualized by Freeze-Etching[1]

ROBERT LEONARD, DAVID W. DEAMER, and PETER ARMSTRONG

Department of Zoology, University of California, Davis, California 95616

Received June 3, 1971, and in revised form January 26, 1972

Amphibian yolk platelets are composed of lipoprotein subunits arranged in an ordered crystalline structure. Freeze-etch electron microscopy of isolated *Xenopus* platelets provides a direct view of the structure of the crystal and aids the interpretation of fracture phenomena in lipoprotein systems. A study has been made both of fracture faces and of faces produced by fracturing and etching following partial dissolution of platelets in electrolyte solutions. In freeze-etch replicas, main body crystals appear to be composed of dimers. Rectangular and semihexagonal patterns are seen in fracture faces. Rectangular patterns are seen also in faces produced by partial dissolution and revealed by fracturing and etching. Dissolution faces with possible semihexagonal patterns are distinct but infrequent. Based on this evidence, a new closest-packing model of platelet structure is proposed using lipovitellin dimers as building blocks, with one molecule of the second major protein component, phosvitin, associated with each monomer of the lipovitellin dimer.

Lipids and proteins are the major structural components of biological membranes. Although the quantitative lipid and protein compositions of numerous membrane species have been described in recent years, the manner in which these molecules are organized into functional lipoprotein complexes within the membrane is still uncertain. One approach to this problem has been to utilize model lipoprotein systems in order to gain insight into possible modes of interaction between lipid and protein molecules. One such system, the proteid yolk platelet from the eggs of certain lower vertebrates, is of considerable interest since it represents a naturally occurring bulk-phase crystalline lipoprotein system (*32*). Furthermore, several workers have speculated that platelet lipoprotein may be involved in the generation of cellular membranes during embryonic development (*15*, *16*, *20*, *21*).

The most extensively studied yolk platelet, that of the amphibian egg, has been found to be a three-dimensional crystalline array of subunits (*1*, *16*, *34–36*). The sub-

[1] Preliminary results were presented at the 1971 meeting of the California Societies for Electron Microscopy in Anaheim, California, and at the 11th annual meeting of the American Society for Cell Biology in New Orleans.

units are composed of two different protein species: phosvitin, a phosphorous-containing protein, and vitellin (*31*). These components may be resolved by treatment with aqueous salt solutions of low to moderate ionic strength (*31*). The lipid comprises about 15 % of the dry weight of the platelet and is present as a complex with the protein, vitellin.

The crystalline arrangement of the lipovitellin-phosvitin subunits in the platelet has been investigated with X-ray diffraction (*12*, *13*), and electron microscopy of sectioned platelets (*1*, *16*, *27*, *35*, *36*). The X-ray studies provided structural data on the unit cell of the X-ray scattering elements within the platelets, and the predicted subunit spacings are in fair agreement with results of the electron microscopic studies. However, neither technique resolves the particles themselves, since X-ray diffraction is an averaging technique and electron microscopy of sections depends on heavy metal staining of unknown structural components. Freeze-etch electron microscopy avoids these problems and seemed to be a useful alternative approach to the resolution of subunit arrangement.

The freeze-etch method[1] has the advantage that it introduces a minimal amount of chemical and physical distortion during specimen preparation for electron microscopy. Application of the freeze-etch technique to the problem of membrane structure has resulted in a wealth of new information. One of the most interesting findings is the clear demonstration of particulate structures associated with membranes having bioenergetic functions such as ion transport (*7*) and phosphorylation reactions (*5*). Although it has been suggested that the particles may represent functional lipoprotein structures within the membrane (*4*, *37*). there is no direct evidence that lipoprotein structures are actually revealed by freeze-etching.

Application of the freeze-etch technique to yolk platelet structure is therefore of interest for two reasons. First, the X-ray parameters of yolk platelet structure offer a test of the freeze-etch method in visualizing subunit structure. Second, details of structure within yolk platelets may be revealed which will extend our knowledge of cellular crystals and lipoprotein systems. We report here our investigations of yolk platelets visualized by the freeze-etch technique.

[1] The term "freeze-etching" is used in this paper as the general name for the preparative technique. All specimens were freeze-fractured prior to etching. The distinction between fracture faces and etch faces is carefully described in the results and discussion.

All platelets illustrated were isolated from fertile eggs of *Xenopus laevis*. Encircled arrows show direction of platinum shadow deposition. Linear arrays of particles are enhanced by sighting along the page at a low angle.

FIG. 1. Sectioned, isolated platelet: aldehyde fixed, osmium postfixed, Epon embedded. Section stained with uranyl acetate – lead citrate. An uninterrupted semihexagonal dot pattern is visible throughout. × 53 500. *Inset*: Higher magnification view of semihexagonal pattern from another sectioned platelet. × 100 000.

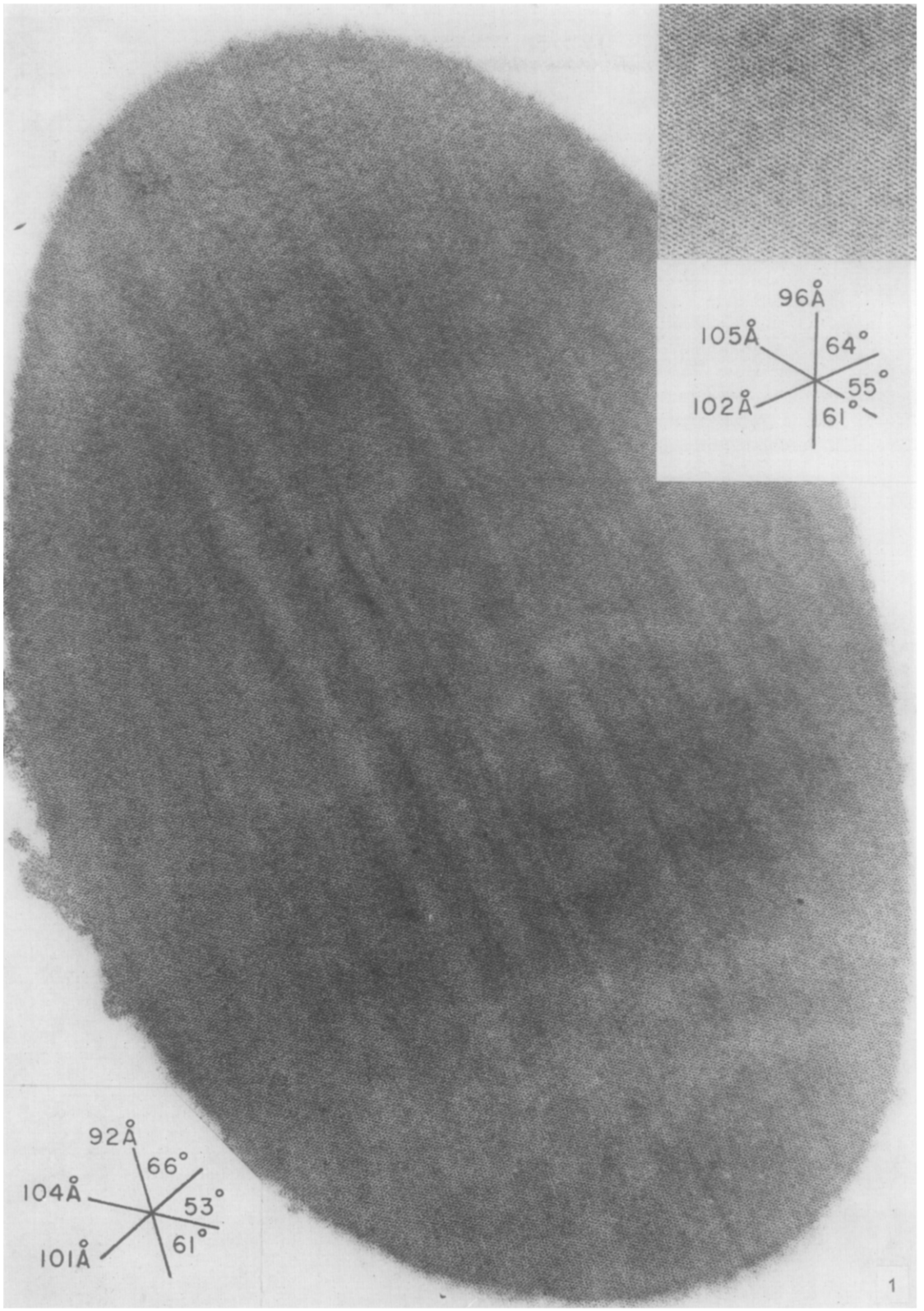
96Å
105Å
64°
55°
102Å
61°
92Å
66°
104Å
53°
61°
101Å

MATERIALS AND METHODS

Platelet isolation. Fertile eggs were obtained from *Xenopus laevis* by mating chorionic gonadotropin (Sigma Chemical Co.)-injected male and female frogs (*11*). All freeze-etch micrographs in this paper are of platelets isolated according to Essner (*9*). Isolated platelets were used immediately or stored up to several weeks in 0.1 M NaCl at 5°C until needed. No obvious deterioration of platelet ultrastructure occurred during storage.

Electron microscopy of sectioned platelets. Isolated yolk platelets were fixed in a cacodylate-buffered glutaraldehyde–paraformaldehyde mixture (*18*, *30*) for 0.5–2 hours at 4°C. Fixed platelets were washed in cold 0.1 M cacodylate buffer and postfixed in a cold 1.2% OsO_4 solution. Material was dehydrated rapidly in acetone or ethyl alcohol and propylene oxide prior to embedding. Embedding was in Epon 812, ERL-4206 (*28*), or an Araldite–Epon mixture (Bojax No. 1A). Silver to gray sections cut with a diamond knife were mounted on Formvar carbon-coated grids and stained with 1% aqueous uranyl acetate and lead citrate (*26*). Electron microscopy was performed with a Hitachi HI-11E microscope. A carbon-replica grating (Ernest Fullam Co.; 28 800 lines/inch) was used to calibrate those plates on which dimensions were measured.

Freeze-fracturing and etching. Single droplets of isolated platelets suspended in 2 M sucrose or distilled water were mounted on 3-mm copper disks and frozen in liquid Freon. Sucrose was used to minimize ice crystal formation. Freeze-etching was performed on a Balzers instrument (*2*, *24*) using unsharpened platinum-alloy razor blades. A standard etching time of 20 seconds at $-100°$ was used in all experiments. Replication was performed by platinum-carbon shadowing followed by carbon reinforcement. Replicas were cleaned for 1 hour or more by flotation on dilute solutions of commercial bleach. Cleaned replicas were picked up on bare 300-mesh grids from distilled water.

The potential for contamination artifacts (*8*) was minimized by the relatively short etching time and protection of the specimen fracture surface by the cold knife during etching. Contamination of fracture and etch faces was not visible in platelet preparations.

Experimental alteration of platelets. Freeze-etch studies of dissolution of platelets in salt solutions (20 mM $CaCl_2$ and 500 mM NaCl) were carried out directly on the copper disks used for mounting and freezing. A small amount of platelet suspension was added to a drop of salt solution on a disk. After 2–5 seconds, when dissolution was partially completed, the disks were plunged into liquid Freon for freezing. Mounted disks were stored in liquid nitrogen until needed for freeze-etching. Sucrose was omitted from solutions used in the salt dissolution experiments.

RESULTS

Sectioned platelets

A sectioned isolated yolk platelet from *Xenopus laevis* is shown in Fig. 1. The limiting membrane and superficial layer are lost during isolation, leaving only the main body crystal (see also Fig. 11). Individual subunits, clearly resolved in Fig. 1 (and inset), are packed in a semihexagonal arrangement.

FIG. 2. Fracture face showing rows of particles in semihexagonal array and intervening linear faces (arrows) each consisting of two parallel lines. Particles have 85 Å spacing along the principal rows with 100 Å repeat distance between rows. In the upper area where rows of particles alternate with intervening faces the principal spacing is 170 Å (see Fig. 15 for diagrammatic interpretation). × 120 000.

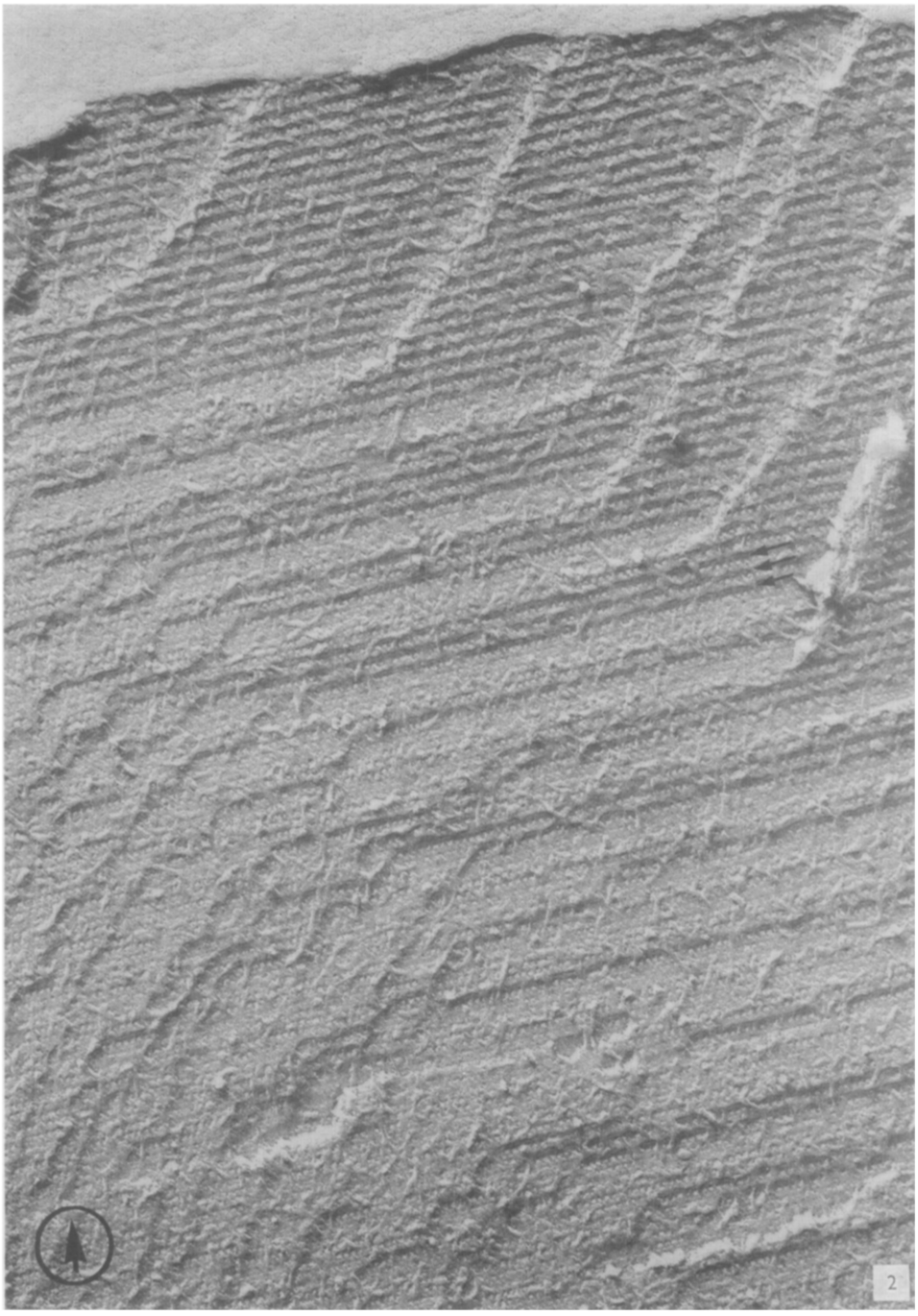
2

Freeze-etched platelets

Isolated platelets, untreated. Replicas of isolated platelets suspended in 2 M sucrose revealed a variety of fracture face images. Figure 2 shows a fracture face with varying quality of detail in different regions. Most of the area reveals structural units with sufficient clarity for measurements of repeat distances. Especially evident are rows of particles or subunits which seem to be part of a basic semihexagonal array. Within the rows, subunits have a uniform 85 Å spacing. Some rows of subunits are separated by narrow intervening linear faces (arrows) which show no evidence of subunit structure but appear, instead, to consist of two parallel lines. At the top of Fig. 2, where linear faces alternate with rows of subunits, the repeat distance is 170 Å. Spacing between rows of subunits (no intervening faces) is 100 Å.

In the lower left area of Fig. 2 note the decreased fracture quality and consequent loss of detail. Here, the fracture plane crosses obliquely through several structural planes in the platelet. As in sectioning, there is no way to control the angle of incidence of the knife blade with respect to the platelet, and thus many platelets are fractured obliquely and show little detail. These regions are usually overlaid by varying amounts of material having the appearance of short, thick fibers which may represent plastic deformation of platelet components during fracturing.

In Fig. 3, the fracture face reveals a rectangular pattern with 85 Å spacing between uniform rows (arrow labeled U) and, in the other direction (at an angle of 89°), lines of alternating intensity with a long spacing of 155 Å (arrow labeled L)[1]. The difference in subunit pattern from that in Fig. 2 suggests that the fractures followed a rectangular plane through the platelet in Fig. 3. The rectangular pattern in Fig. 4 is tilted out of the plane normal to the line of sight (probably due to tilt of the specimen in the electron microscope) resulting in a decrease in uniform spacing to 70 Å,

[1] The following terminology will be used here to describe rectangular patterns: long spacing (between L rows) refers to the repeat distance between alternating lines of like shadow intensity; uniform spacing (between U rows) refers to the repeat distance between rows of subunits that do not alternate in intensity.

FIG. 3. Fracture face showing rectangular pattern of particles. Rows designated by arrow "U" have a uniform 85 Å spacing. Rows ("L") that alternate in shadow intensity form an angle of 89° with the uniform rows and have a long spacing of 155 Å. × 134 000.

FIG. 4. Rectangular pattern in fracture face oriented as in Fig. 3 but with enhanced alternation of shadow intensity between the "L" rows. Long spacing is 155 Å; uniform spacing, at an angle of 80°, is 70 Å. Distortion of the angle from 90° to 80° and decrease in spacing are probably due to tilt of the specimen in the microscope. × 134 000.

FIG. 5. Semihexagonal pattern of particles. Inset shows angles between linear arrays of particles and spacing between particles. Note the presence of material that obscures detail in the fracture face. This may be due to plastic deformation of platelet components during fracture at −100°C. × 134 000.

FIG. 6. Fracture face (*F*) showing parallel crevices penetrating the platelet interior due to the action of $CaCl_2$ solution prior to freezing in Freon. Structural pattern is discernible in the crevices. The pattern of particles in the fracture face appears semihexagonal. × 134 000.

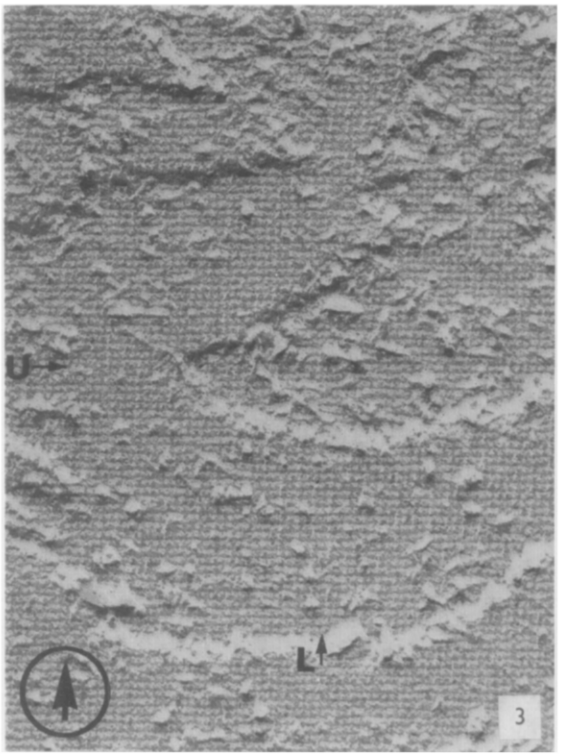
U
L
3

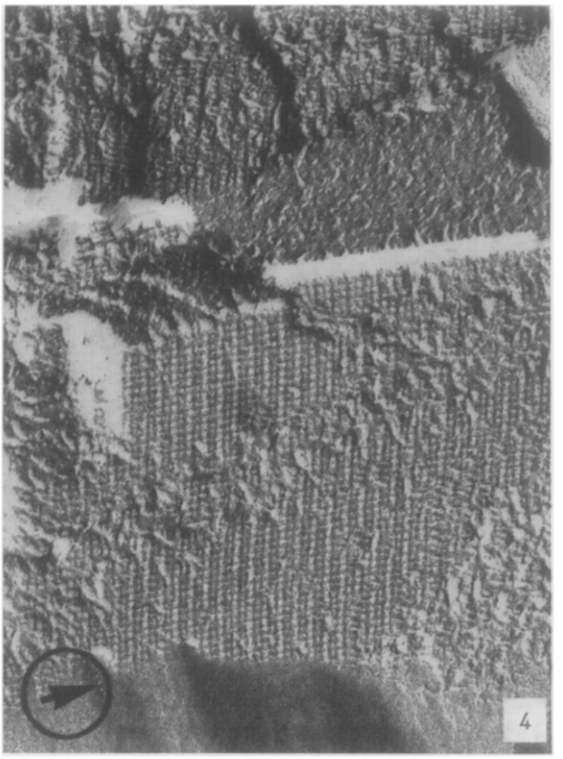
4

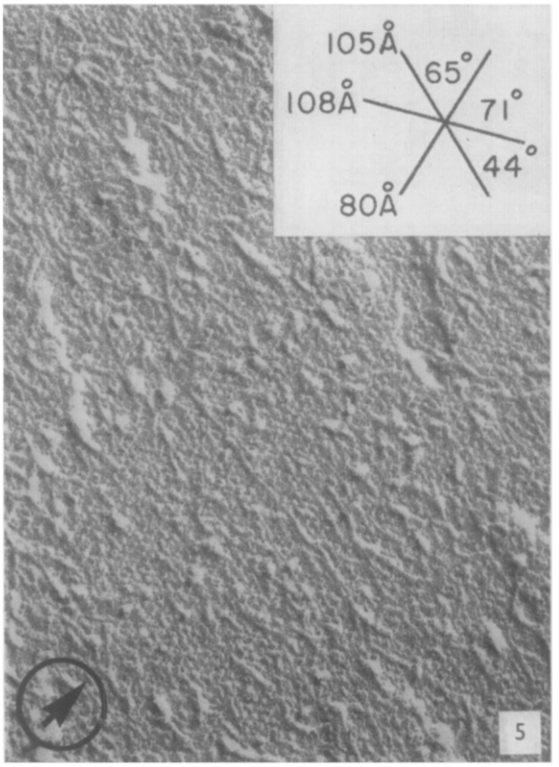
105Å
65°
108Å
71°
44°
80Å
5

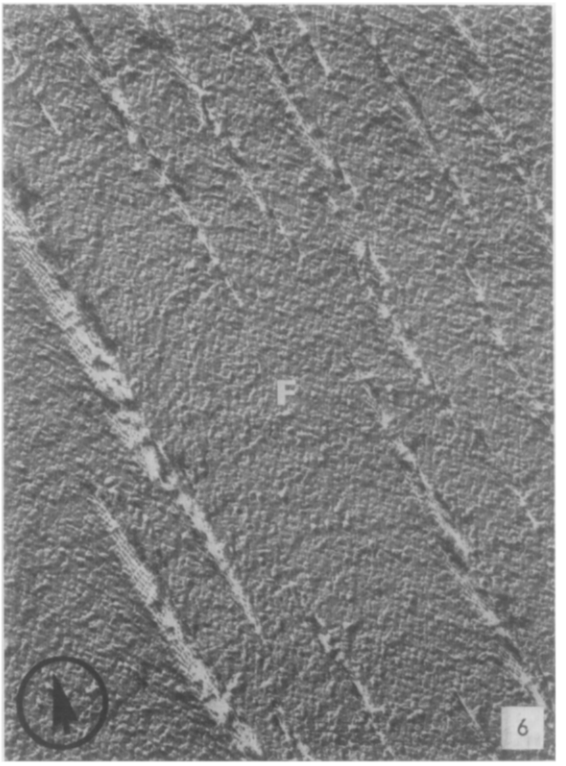
F
6

TABLE I

ANGLES MEASURED IN "HEXAGONAL" ARRAYS IN SECTIONED YOLK PLATELETS OF VARIOUS ORGANISMS[a]

Organism	Angles (3 per array, in degrees)	Reference
Rana esculenta	55, 61, 64; 48, 60, 72 49, 62, 72	(*22*)
Rana pipiens	53, 58, 69 49, 64, 67	(*16*) Armstrong (unpubl.)
Triturus pyrrhogaster	54, 58, 68 50, 63, 67	(*13*) (*16*)
Ichthyomyzon, Petromyzon (Lamprey)	48, 56, 76	(*17*)
Xenopus laevis	53, 61, 66; 55, 61, 64 61, 71, 48	Fig. 1 (*1*)

[a] Perfect hexagons have 60° angles only.

and a distortion of the angle between the long spacing rows and the uniform rows to 80°. There is a marked enhancement of the long spacing (155 Å) pattern of alternating heavily shadowed and lightly shadowed subunits.

Subunits are arrayed in imperfect hexagons (semihexagons) in Fig. 5. Angles between rows of subunits depart appreciably from the 60° expected in perfect hexagons. Some of the angular and spacing variation is probably due to tilt of the specimen (see discussion). Angular deviations from 60° are also observed in sectioned material (Table I). Fracture faces exhibiting similar semihexagonal arrays are common in the replicas but resolution of subunits is never as clear as in the rectangular arrays shown in Figs. 3 and 4.

Calcium chloride and sodium chloride dissolution of isolated platelets. Platelets dissolve in $CaCl_2$ solutions of low concentration (20–50 m*M*) (*9*, *10*, *29*) and in NaCl solutions of higher concentrations (500 m*M*) (*9*). The beginning stages of dissolution were captured by rapid freezing with the hope that the faces revealed in this process would provide structural images of platelet interiors to complement fracture face images. Detailed ultrastructure is indeed visible in such preparations after freeze-etching. Dissolution proceeds by the formation of narrow elongated crevices that penetrate deep into the interior of the platelet (Fig. 6). These crevices seem to follow

FIG. 7. Large fracture area showing identical structural patterns in dissolution faces (*D*) revealed by etching of ice (*I*) and in fracture faces (*F*). Note disruption of structure in the region of the arrow and several other parts of the dissolution faces. × 32 000.

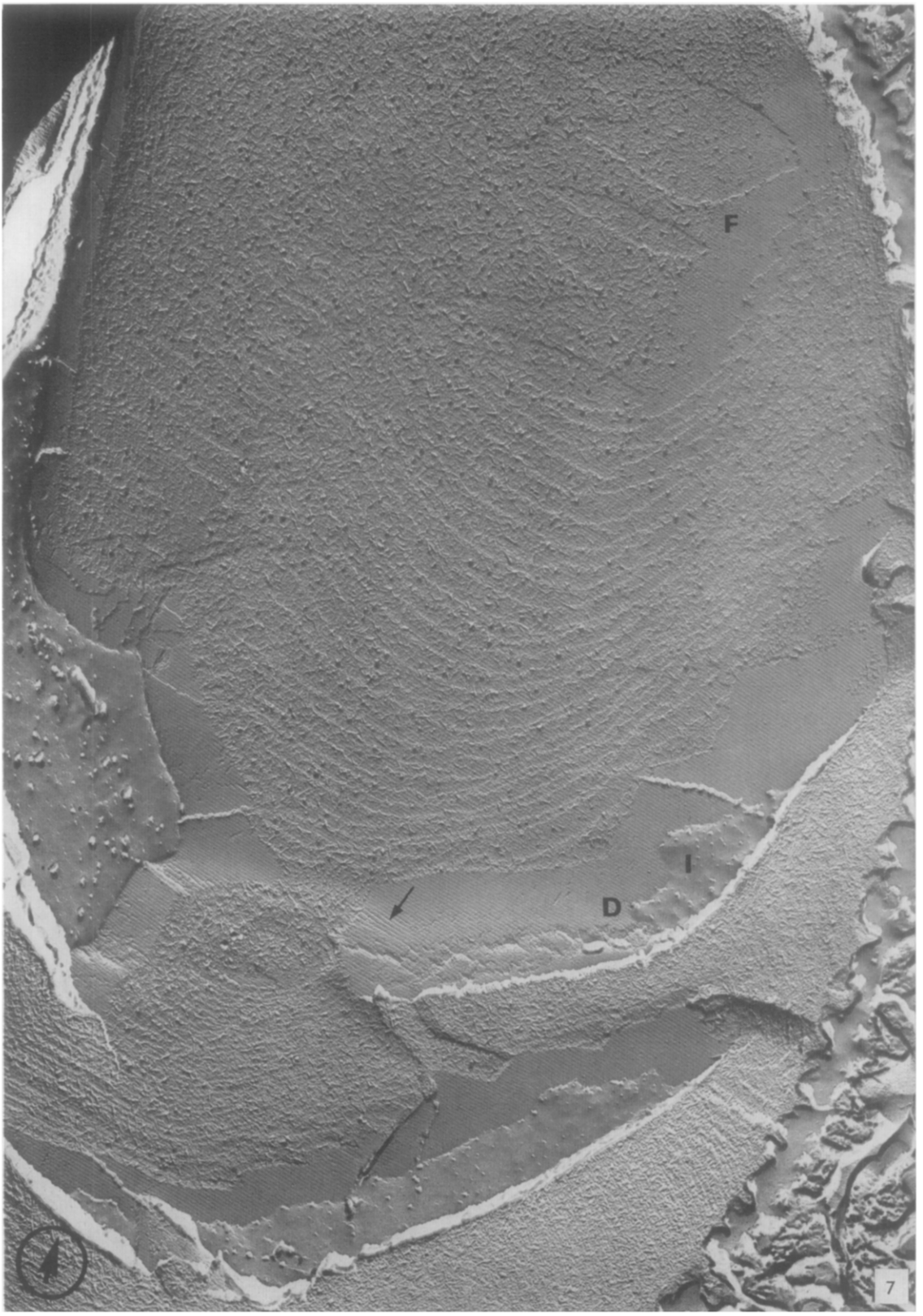
F
I
D
7

TABLE II

COMPARISON OF LATTICE SPACINGS DERIVED FROM X-RAY DIFFRACTION AND ELECTRON MICROSCOPY

Structural pattern	Spacing		
		Electron microscopy	
	X-ray diffraction (*Rhacophorus*)	Freeze-etch (*Xenopus*)	Sections (*Xenopus*)
Hexagonal or semihexagonal	110	80 to 108	92 to 105
Rectangular	110 × 200[a]	85 × 170	Not seen in amphibians (85 × 85 in lamprey)

[a] Estimated from the model, Fig. 13B.

definite structural features in a platelet since their long axes lie parallel to each other, rather than showing a random orientation. In some platelets, crevices were observed at approximately 60° angles to the principal parallel series. Patterns on these infrequent faces (Fig. 10A and B) seem to be more complex than the common rectangular patterns (Figs. 6–9). From the orientation we would expect them be semihexagonal views but tilt effects have thus far precluded a satisfactory analysis of the patterns.

In Fig. 6 the planes of dissolution angle steeply away from the surface of the fracture face. The fracture plane in Fig. 7 was more nearly coplanar with the face of a dissolution crevice. Here, fracture occurred through the ice (*I*) in the crevice (above face *D*) as well as through intact crystal (upper half of the figure). Subsequent etching away of the ice revealed the underlying face of the dissolution crevice. In this picture, platelet subunits are visible both in the fracture faces (*F*) and on the faces of the dissolution crevices (*D*). Remnants of ice (*I*) on the latter faces demonstrate the prior presence of dilute salt solution in the crevices and provide a distinct marker for dissolution faces. Basic subunit patterns on both types of faces are identical despite the fact that the faces were formed by very different physical processes. Slight curvature of the faces and rows of subunits on the dissolution face (arrow) further attest to the action of the salt solution. Fracture faces never show distortions of structure of this nature.

A higher magnification view of a dissolution face is shown in Fig. 8. The rectangular pattern derives from rows of paired subunits. The pattern and spacing here are

FIG. 8. Rectangular array of distinct subunits in a dissolution face revealed by etching. Long spacing is 170 Å. Uniform spacing is 85 Å. Angle between linear arrays is 87°. Subunits appear to have been dislodged from the lattice in many places. × 128 000.

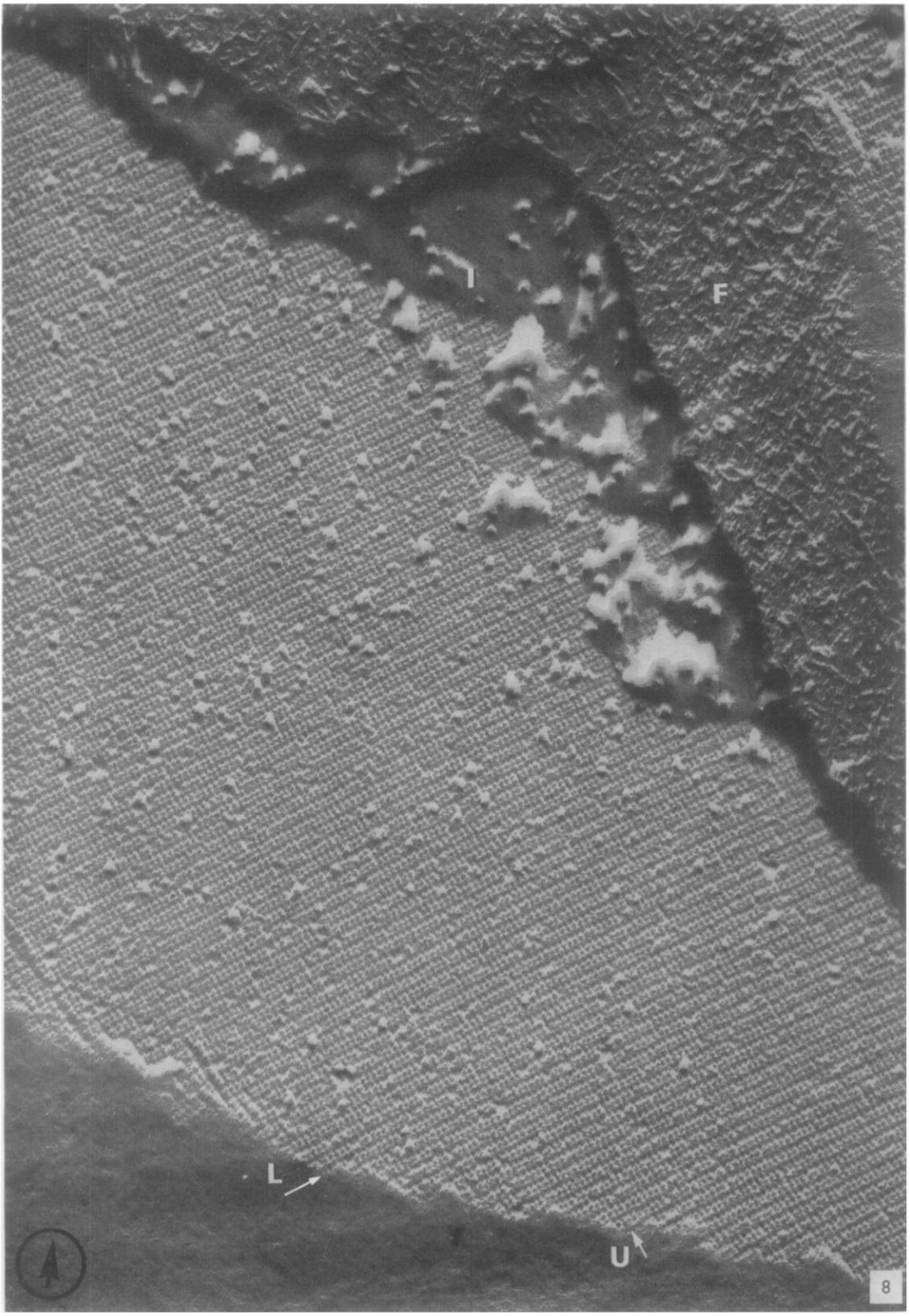
I
F
L
U

characteristic of all rectangular faces revealed by $CaCl_2$ dissolution and apparently represent the same structural planes as those in Figs. 3 and 4. It should be noted that long spacings in the fracture faces of Figs. 3 and 4 are 155 Å while the long spacings in the dissolution faces of Figs. 8 and 9 are 170 Å. These discrepancies in long spacing are probably due to specimen tilt and thus do not rule out the identity between rectangular patterns in fracture and dissolution faces, particularly in light of Fig. 7 which shows both types of faces in the same platelet.

Another dissolution face is shown in Fig. 9A. The lower left area has a subunit pattern identical with that of Fig. 8. However, the pattern changes beyond the step (arrows); intense white (unshadowed) lines predominate instead of black lines. These two distinct shadow patterns appeared frequently in both fracture and dissolution faces and are highly significant. They will be discussed later in relation to the arrangement of protein constituents of platelets.

The etch face in Fig. 11 shows the exterior surface of a main body platelet crystal. The rectangular pattern is identical to internal dissolution and fracture face patterns. Such arrays are, of course, revealed only in certain orientations of the crystal. Semihexagonal patterns were never observed in etch faces of the external surface of the main body crystal.

All of the dissolution faces shown above were produced by $CaCl_2$ dissolution. Studies of Gross (*10*) suggested that differences exist between the mechanisms of dissolution by $CaCl_2$ and NaCl solutions. The present studies provide no evidence for different mechanisms, since freeze-etched dissolution faces produced by NaCl appear identical in every detail to those produced by $CaCl_2$.

Effects of chemical fixation and dehydration on platelet images. Glutaraldehyde and osmium fixation and dehydration of platelets were attempted during this study in the hope that additional information might be obtained on the structural relationships between lipids, proteins, and water. Results were not sufficiently clear to warrant a detailed account but general effects are of interest. Both types of fixation prevented clear resolution of subunits although definite fracture faces still resulted. Fixation also prevented the appearance of fibrous texture on fracture faces. This is evidence for physical restriction of plastic deformation of the crystal lattice at the time of fracture. That material can be bent or pulled from the unfixed crystal at such low temperature suggests that the "frozen" lipid–protein–water system is neither

FIG. 9. (A) Dissolution face with a rectangular array similar to Fig. 8 but showing two different shadow patterns. Black lines are most distinct to the left of the step designated by the arrows; white lines dominate on the right. ×130 000. (B) A single layer of tilted dimer subunits (see model, Fig. 12) gives a simulated shadow pattern similar to the area directly above in Fig. 9A. Lighting is at 45° from the left. (C) With the model reversed in the same lighting the shadow pattern corresponds to the right-hand area of Fig. 9A. Shadows in the model correspond to deposits of platinum in the freeze-etch replica.

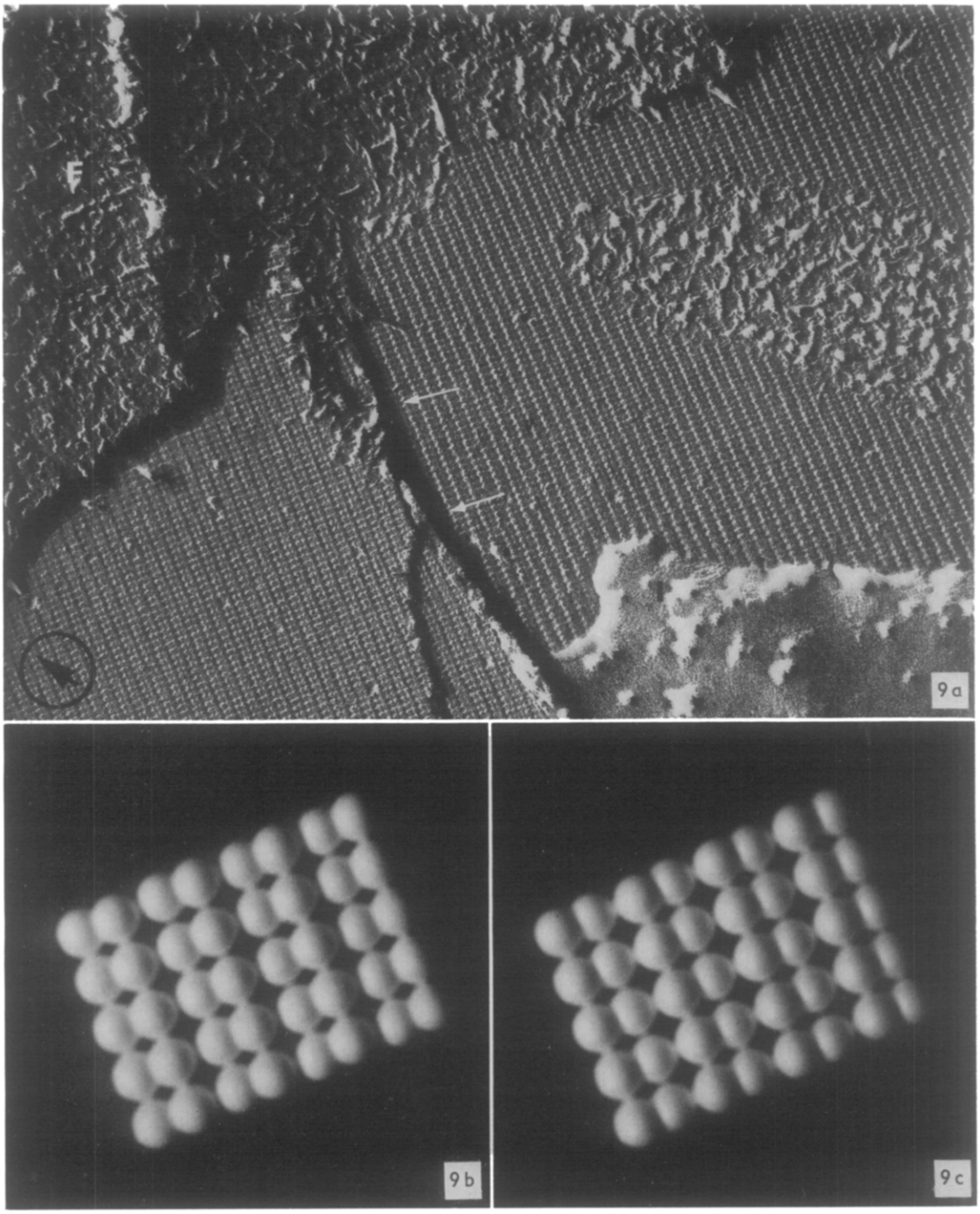
F
9a
9b
9c

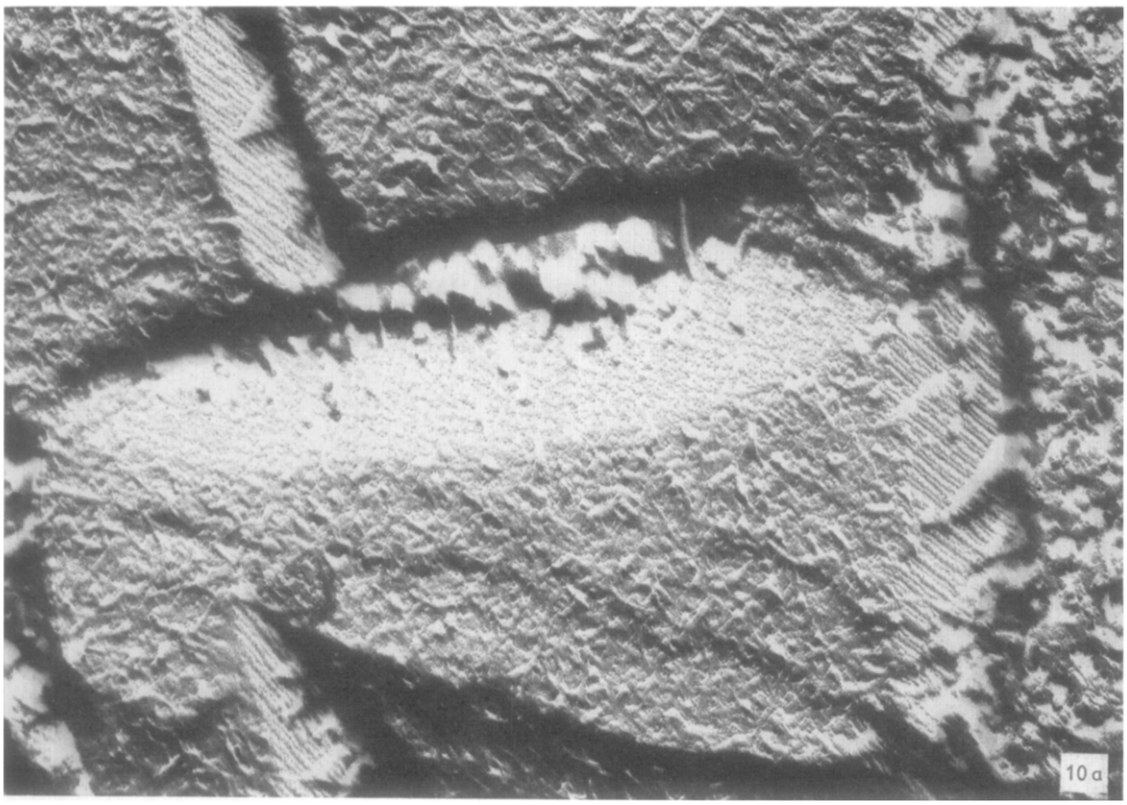

10 a

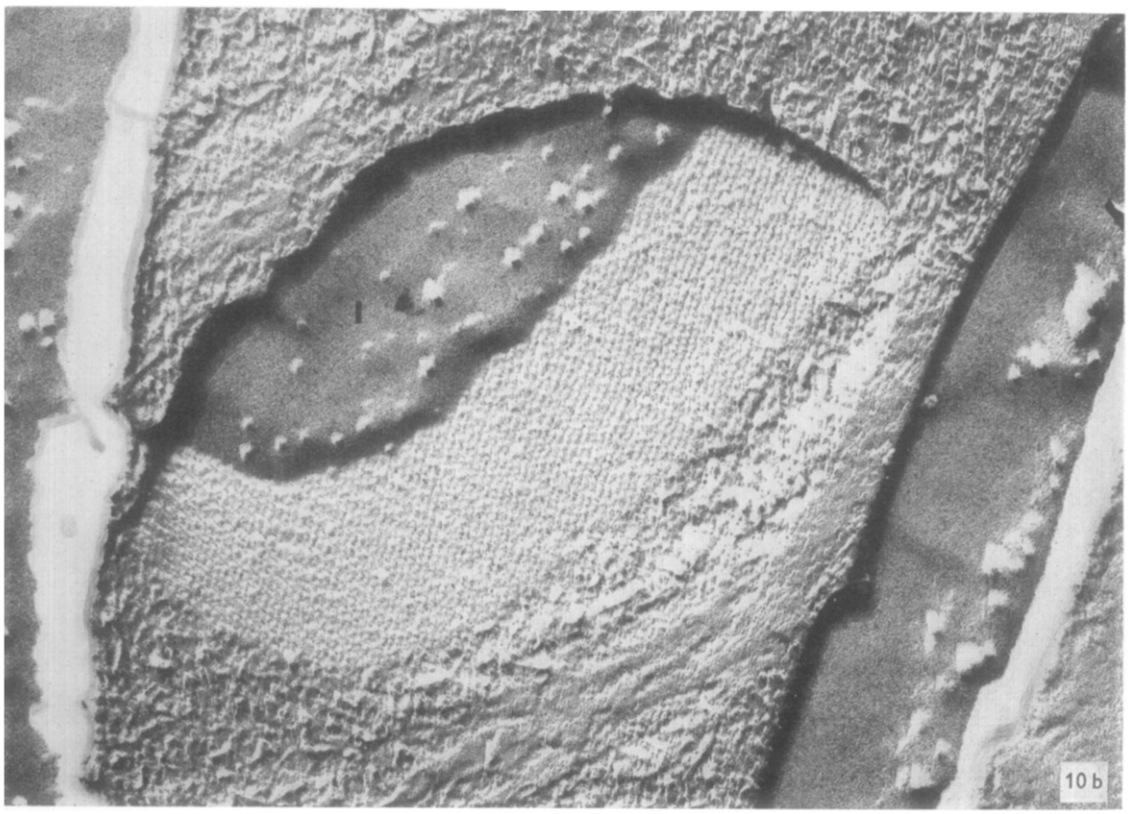

10 b

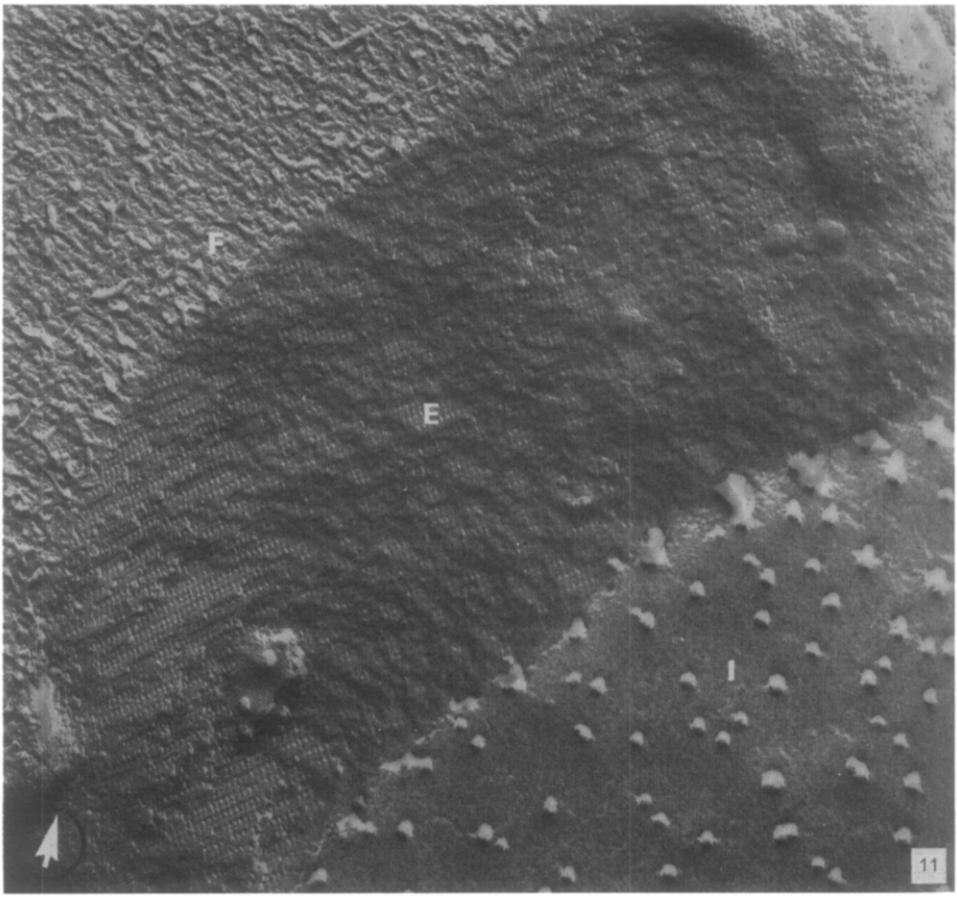

FIG. 11. Etch face (*E*) of the outer surface of a main body platelet crystal mounted in distilled water. Retreating ice front (*I*) is at lower right. The rectangular pattern appears identical to those in internal fracture and dissolution faces. ×110 000.

brittle nor rigid. Glutaraldehyde fixation of membranes does not seem to interfere with normal fracture morphology (*5*, *6*) whereas osmium fixation greatly decreases the frequency of membrane fracture faces in *Mycoplasma* (*14*). Both glutaraldehyde and osmium fixation make platelets resistant to $CaCl_2$ and NaCl dissolution.

FIG. 10. (A) A second type of dissolution face, seen infrequently, showing a pattern that may be semihexagonal. Note that this dissolution crevice follows a plane different from the adjacent crevices that show rectangular patterns. (B) Dissolution face showing subunit pattern more clearly, and patch of ice (*I*) within the crevice. (A) ×117 000; (B) ×117 000.

Dehydration of unfixed platelets either by lyophilization or by organic solvent treatment resulted in almost complete loss of structural fracture planes. Water is undoubtedly involved in platelet structure and may well influence lipids and proteins through hydrophobic–hydrophilic interactions.

DISCUSSION

Freeze-etch electron microscopy of yolk platelet crystals provides a unique view that complements reports based on X-ray diffraction, biochemical analysis, and electron microscopic observation following chemical fixation, dehydration, embedding, and sectioning. The present study has established that freeze-fracture and freeze-etching can resolve subunits of structure in yolk platelets. To our knowledge, this is the first crystalline lipoprotein system to be characterized by this method. The images obtained are not completely consistent with the general dimensions of the lattice model developed from X-ray diffraction data (*12*, *13*) and, as will be detailed below, the lattice structure itself appears to differ significantly from that model.

Sources of error

Dimensions, spacings, and angles derived from electron micrographs are subject to errors arising from tilt of the section or the freeze-etch replica with respect to the plane normal to line of sight (electron beam). The projected image of a tilted specimen will show decreased spacings and/or obscured detail. Karasaki (*16*, *17*) described tilt effects in sectioning studies of platelets. In that study, intentional slight tilting of sectioned specimens showing hexagonal arrays produced band patterns rather than distorted hexagons. Band patterns do not occur in tilted freeze-etch replicas because their extreme thinness preserves the image of discrete subunits. However, the subunit spacings and angles are distorted. Tilt in a replica can occur not only on the microscope stage but in the fracture face itself because of its three-dimensional nature. Since tilt causes a decrease in the observed spacing, the maximum measured spacings would most closely approach reality. Distortion of the angles between linear arrays of subunits is seen in Fig. 4. These angles should be 90° in rectangular patterns but are here distorted to 80°. There is a corresponding decrease in spacing in one direction to 70 Å. The 155 Å long spacings in both Figs. 3 and 4 are low compared to those in Fig. 8, probably as a result of tilt. Since tilt probably affects most replicas to some extent, only maximum spacings and the angles in rectangular arrays yield reliable quantitative structural information.

Tilt effects on semihexagonal array angles and spacing cannot be evaluated as easily due to the uncertainty of the true dimensional parameters (i.e., subunit spacings and angles between rows of subunits). Even so, it is significant that perfect

hexagonal arrays of subunits have never been observed, either in sectioned material (Table I) or freeze-etched platelets (Fig. 5). This apparent lack of perfect hexagons probably reflects a real structural variation from a perfect hexagonal lattice, and not simply distortion arising from tilt.

Distortion may also result both from freezing and from fracturing. Gross freezing damage (ice crystal formation) was avoided through use of cryoprotective agents (2 M sucrose). It is impossible to judge whether more subtle distortion occurred during freezing. Fracture may also result in distortion of platelet fine structure due to compression or plastic deformation. The production of fibrous material on fracture faces is evidence for small-scale plastic deformation. Fracture damage is not present in dissolution faces, but here too, some disarrangement of structure may occur (viz. the curved rows of subunits in Fig. 7, arrow).

Yolk platelet crystal structure

Fracture and etch face images. The patterns seen in freeze-fracture faces result from the tendency of fracture planes to follow structural planes within the platelets. The orientation of most platelets is such that fractures cross many planes obliquely and reveal little fine structural detail. Among the many variations in fracture patterns, the rectangular and semihexagonal are the only two patterns that are clearly definable in terms of subunit spacing and angles between linear arrays of subunits.

One of the interesting features of *Xenopus* yolk platelets is the fact that identical rectangular patterns are revealed both by fracture and by dissolution in salt solution. The patterns on the faces of dissolution crevices are extremely clear because of minimal structural disruption at the time of fracture. Rectangular patterns are nearly as clear in fracture faces.

Freeze-fracture may involve the separation of lipid tails from sites of insertion in the vitellin dimers. Fracture would thus be expected to cause greater disruption of structure than separation of hydrophilic lipid polar groups or hydrophilic segments of protein subunits during dissolution in weak ionic solution. In any case, resolution by platinum shadowing is not sufficient to reveal the true position of the relatively small amount of lipid present in the yolk platelet. In support of this contention is the fact that fracture faces of membranes do not show morphological features attributable to lipid alone, in spite of the high percentage of lipid present in the membrane interior (*3*, *8*).

It is reasonable to infer that lipid is partly responsible for the difference in quality of fracture between rectangular and semihexagonal arrays. If both types of array involved the same kind and strength of association between lipids and proteins, we would expect identical resolution of arrays after fracture and after salt dissolution.

This identity is not borne out: semihexagonal arrays do not fracture cleanly, and they appear infrequently in dissolution faces.

Sectioned platelet images. Thin sectioned platelets show a variety of images of the main body crystalline material, including unordered granular areas and ordered arrays of lines or dots (Fig. 1). Apparently the granular and line images are the result of tilt of a basic dot pattern of platelet subunits (*17*). It might seem surprising that subunits are resolved in sectioned material at all since thin sections averaging 300–500 Å in thickness would contain several in-focus layers of electron dense particles (probably phosvitin molecules). In most orientations of the platelet, each layer would be expected to obscure the interstices in adjacent layers. One suggestion which has been made is that enhancement of electron density with heavy metal staining of sections is affecting only the surface layers of particles in the sections (*17, 23*). However, recent studies of stain penetration into sections provide strong evidence that sections are stained throughout (*19, 25*). As will be discussed in more detail later, subunits in semihexagonal array are in register in one direction in the model which we have derived from the freeze-etch data (i.e., when the crystal is viewed in side-view, as in Fig. 14A). Sections normal to lines of subunits in register would show the subunits in semihexagonal array.

Both rectangular and hexagonal arrangements of particulate subunits have been reported in micrographs of lamprey egg platelets prepared by staining and sectioning (*17*). In the lamprey, rectangular patterns are extremely clear; semihexagonal patterns are less clear but definite. These differences in pattern clarity parallel those in freeze-etched *Xenopus* platelets. Lack of stability in salt solutions and the apparent absence of rectangular patterns in sectioned amphibian platelets led Karasaki to "suggest a higher order of macromolecular close-packing" in lamprey platelets. Although rectangular patterns in freeze-etched amphibian platelets are clearly illustrated in the present study, the absence of such patterns in sectioned material suggests a real difference in crystal structure between the two organisms.

Previous models. The basic goal of the present study is to examine the nature of the crystalline packing of yolk platelet subunits. Amphibian yolk platelets consist of crystalline lattice arrays of the protein molecules, phosvitin and vitellin, lipid molecules, and water (*32*). A simple hexagonal lattice was proposed by Wallace (working with *Rana pipiens*) as a model for this array based upon considerations of molecular volumes, birefringence of platelets, and band and dot patterns seen in electron micrographs of sectioned material. On the basis of X-ray analysis of platelet structure in the frog, *Rhacophorus*, Honjin et al. (*13*) proposed a new model in which the phosvitin molecules are arrayed in a hexagonal crystal lattice with an observed axial ratio of 2.1. The unit cell contains 3 component protein units in lattice positions that were assumed to involve closest packing of oblate spheroids. Both hexagonal models

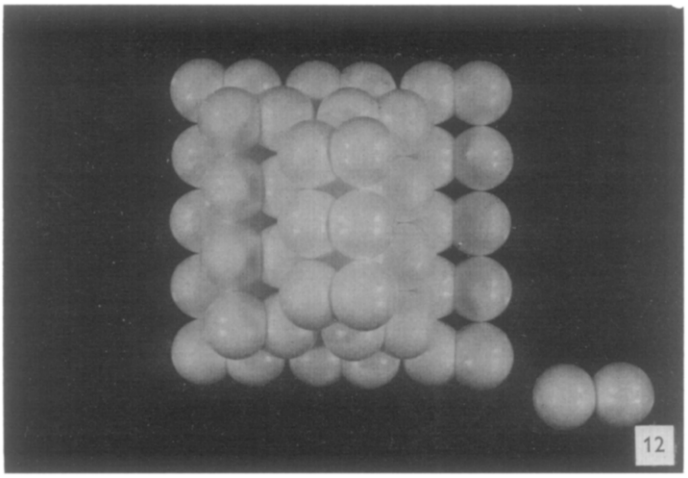

FIG. 12. Photograph of a new freeze-etch model of amphibian yolk platelet crystalline structure. Building blocks are pairs of spheres bonded together on small flattened areas to form "dimers" (inset) representing the platelet component lipovitellin. Each lipovitellin dimer presumably contains two phosvitin molecules. The dimers stack in a stable, closest-packed structure. Layers coplanar with the photograph are composed of rectangular arrays of dimers. Dimers in a given layer tilt in nesting with adjacent upper and lower layers which have opposite but equal tilt (see Figs. 9B and C).

describe the basic lattice structure in terms of the phosphoprotein which is believed to impart the principal electron and X-ray scattering properties to the platelet. Lipid and vitellin are arranged arbitrarily around (*13*) or next to (*34*) the denser protein. Water is believed to fill the molecular interstices in some as yet undefined way.

Model derived from freeze-etch images. The present freeze-etch images strongly support a suggestion by Wallace and Dumont (*34*) that the lipovitellin molecule is a dimer. These investigators were able to split the 400 000 molecular weight molecule into two 200 000 molecular weight subunits at high pH. Wallace (*33*) has provided evidence for a close structural and chemical relationship between yolk platelet subunits and vitellogenin, the apparent direct precursor of the platelets in *Xenopus* ovarian tissues. Vitellogenin is transported to the oocytes from its site of synthesis in the liver as a component of blood serum. It is plausible that the hypothesized vitellogenin dimer, which contains two phosvitin molecules, is the dimer seen in freeze-etch preparations of the platelets themselves. Earlier biochemical data obtained by Wallace (*31*) had shown the phosvitin to exist in a molecular ratio of 2: 1 with the lipovitellin. It is reasonable to suggest that the lines of alternating shadow intensity in micrographs such as Figs. 4, 8, and 9 are rows of lipovitellin dimers. These results have led us to propose a modification of the X-ray model (Fig. 12) which incorporates this concept. Here, in contrast to earlier models, lipovitellin dimers are

the structural units (Fig. 12, inset), rather than phosvitin molecules. In our model, one phosvitin molecule is assumed to be associated with each monomer of the lipovitellin dimer.

The hexagonal model derived from X-ray data is pictured in Fig. 13A. This is reproduced from Honjin and Nakamura (*12*) and can be compared with a scale reconstruction (Fig. 13B) which presents a modification of the X-ray model based on our freeze-etch data. In the reconstruction, balls represent the centers of the lipovitellin monomers (MW 200 000) described by Wallace and Dumont (*34*), while in the drawing of Honjin and Nakamura (Fig. 13A), the spheres represent the positions of phosvitin molecules. The proposed arrangement of lipovitellin dimers (MW 400 000) in the model has been indicated by the pairing of shaded balls. The positions of two lipovitellin dimers (comprised of 4 monomers) are shown in Fig. 13B. Note that planes of dimers are at angles to the hexagonal planes of the model. The dimensions of the X-ray model are $a=b=110$Å and $c=240$ Å. When these are inserted into our scale model, they result in a center-to-center spacing between monomers in the dimer of approximately 100 Å. This would suggest a dimer having end-to-end dimensions of about 200 Å. This is larger than the observed 170 Å long spacing distances in Figs. 8 and 9. (The long-spacing distance is a measure of the length of the dimer in the rectangular plane; see Figs. 4, 7, 8, and 9A.)

Several factors may contribute to the discrepancy in dimensions. Generic differences may be important. Hexagonal dimensions for *Rhacophorus* (the genus used in the X-ray studies) are larger than for the genus used by us (*Xenopus*); see Table II. In addition, the X-ray measurements were performed on fresh material, while our material was frozen. Both factors could be evaluated if X-ray data of frozen *Xenopus* platelet material become available.

The most important difference between the X-ray and freeze-etch model is the distribution of molecular weight within the crystal structure. The subunit of Honjin's X-ray model is a fused phosvitin dimer surrounded by an oblate spheroid of vitellin of molecular weight 400 000 [see Fig. 10 of (*13*)]. In the freeze-etch model, the two phosvitins and the 400 000 MW of lipovitellin are distributed in two monomers, each containing one phosvitin and 200 000 MW of lipovitellin. Thus, our model would be roughly half as dense as the X-ray model if the *a*, *b*, and *c* distances were maintained. However, as is mentioned above, these dimensions appear to be smaller in frozen *Xenopus* platelets than in fresh *Rhacophorus* platelets.

It is of interest to compare our model to the images seen by electron microscopy of sectioned material. As noted previously, dot patterns in semihexagonal array have been noted in amphibian platelets. This result is consistent with our freeze-etch model in that subunits are in register along axes normal to the planes showing semihexagonal packing of subunits (Fig. 14A). It is of further interest that particulate subunits are

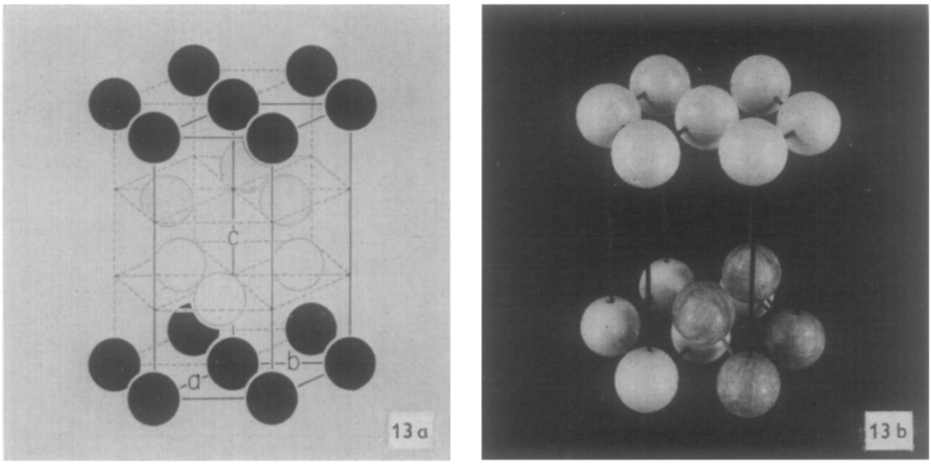

FIG. 13. (A) Reproduction of Fig. 4 (*12*), X-ray model of main body yolk platelet crystal structure in *Rhacophorus*. (B) Scale reconstruction of the first, fourth, and part of the second tiers of the X-ray model showing suggested pairing of lipovitellin monomers (MW 200 000) to form the lipovitellin dimer (MW 400 000) with center-to-center spacing of approximately 100 Å. Only two pairs of balls are shaded, and one member of the second tier and the entire third tier of subunits have been left out to clarify orientation in the crystal model. In Fig. 13A, each ball represents the center of the lipovitellin dimer, while in Fig. 13B each ball represents the position of the center of a lipovitellin monomer, with pairs of connected shaded balls representing the dimer positions.

never seen in thin-sectioned amphibian material in rectangular patterns [although rectangular "line" patterns have been reported; see Fig. 4 of reference (*13*)]. This is consistent with the freeze-etch model since subunits are not in register along axes normal to rectangular planes (see Fig. 12). Karasaki has reported rectangular patterns of discrete subunits in sectioned lamprey platelets (*17*). This observation suggests that the lamprey and amphibian platelets are structurally different.

The best freeze-etch evidence for dimer subunits is seen in alternating lines of shadow deposition in rectangular patterns such as Figs. 4, 8, and 9A. The two distinctly different rectangular patterns seen in different parts of the same platelet in Fig. 9A are coplanar and have identical spacings. The pattern difference between the two areas can be accounted for in the dimer model, photographed in a single layer in Figs. 9B and C. When dimers are packed in a closest-packing arrangement, tilting of dimers in the dimer (rectangular) plane is automatically introduced if the monomers are flattened where they adhere to one another. In a multilayered model, the dimers tilt uniformly in each layer with the tilt alternating from one layer to the next. The angle of tilt of dimers depends upon the degree of flattening of monomers where they are fused into the dimer. Deviation introduced into the present model (i.e., flattening of appressed sides) is constant but arbitrary since the exact shape of the

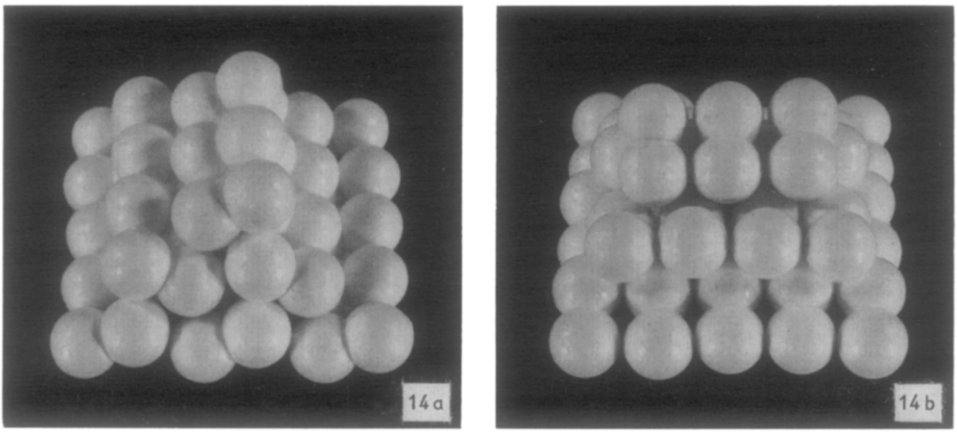

FIG. 14. Oblique views of the dimer model showing semihexagonal arrays. There are four planes through the lattice containing semihexagonal arrays, but there are no perfect hexagonal arrays as in the X-ray model (Fig. 13). Two of the semihexagonal planes are identical "side views" (A) of the dimers. The other two planes are identical "end views" (B). Resolution of semihexagonal patterns in both sectioned and freeze-etched material is too poor to distinguish clearly between the end and side views in micrographs.

subunit is unknown. However, the tilt effect qualitatively explains the appearance of the two different shadow patterns. Figs. 9B and C show by photographic simulation in the model that alternating layers with opposite subunit tilt yield shadow patterns similar to those in Fig. 9A. Note heavy alternating black lines in Fig. 9B. White lines are more intense in Fig. 9C and correspond to linear regions in the platelet etch face that received little or no platinum deposition behind upraised ends of dimers.

Figure 14 gives oblique views of the model to emphasize planes that reveal semihexagonal arrays. When the building blocks are pairs of subunits as in this model, perfect hexagons do not exist in any plane. Planes containing subunits packed in semihexagonal arrays have two possible structural patterns (denoted as side view, Fig. 14A, and end view, Fig. 14B, depending on whether dimers are seen in side view or in end view) but tend to fracture poorly, making it difficult to see detail clearly. Possible semihexagonal arrays (Fig. 10A and B) were seen very infrequently in dissolution faces indicating that those structural planes are resistant to ionic disruption as well as to fracture. This has made it difficult to assign different fracture patterns exhibiting semihexagonal subunit orientation to end-view or side-view arrays. However, it is possible that the differences between the semihexagonal patterns shown by Figs. 2 and 5 may be a result of this aspect of structure with Fig. 2 being an end-view array (see Fig. 14B) and Fig. 5 being a side-view array (see Fig. 14A). As suggested

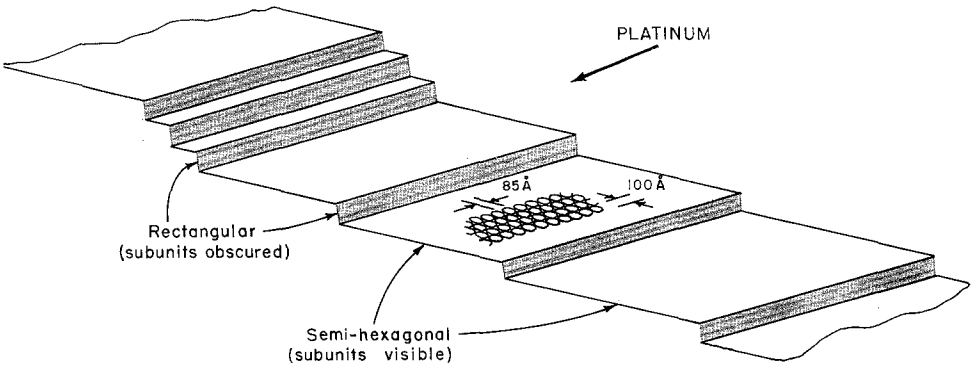

FIG. 15. Diagrammatic interpretation of the pattern seen in Fig. 2. The pattern is semihexagonal where subunits are clearly visible in the micrograph. Narrow faces that do not show subunits were probably oriented so as to receive face-on deposition of platinum which covers rather than resolves detail.

earlier, stained sections showing semihexagonal patterns (Fig. 1) are most likely "side views" since, at least according to our model, this is the only plane in which deeper-lying layers of subunits are viewed in register.

Our interpretation of Fig. 2 is that it is the result of fracture that revealed both semihexagonal and rectangular faces in a series of alternating steps. Linear rows of subunits are in a plane of semihexagonal array; narrow intervening (rectangular) faces consist of two lines and seem not to be composed of discrete subunits. Figure 15 shows this explanation of Fig. 2 in terms of the model. The dominant parallel fracture lines are probably coincident with the lines of alternating intensity in the clear rectangular patterns (e.g., Fig. 8). However, the platelet was so oriented when fractured that only semihexagonal subunit arrays were shadowed at an angle and resolved. The apparent lack of subunits in the intervening faces is due to "face-on" deposition of platinum and resulting filling-in of structural detail.

The freeze-etch model of platelet structure derives from direct visualization of structural elements assumed to be lipovitellin dimers. Formation of platelet crystals and their ultimate dissociation during embryogenesis may involve the dimers as building blocks. The associated phosvitin molecules necessarily assume lattice positions dependent upon the dimers. Nevertheless, it is conceivable that crystal structure as derived from X-ray analysis will differ from results of freeze-etching since different structural elements are "seen" by the two methods: lipovitellin by freeze-etching, phosvitin by X-ray diffraction.

X-ray studies of frozen platelets of the several genera discussed are essential to resolving discrepancies in lattice spacing and problems of hydration and temperature effects on crystal structures and dimensions. Freeze-etching studies with other genera are in progress.

This study was supported by National Science Foundation grants No. GB-23187 (D.W.D.) and GB-30751 (P.B.A.) and by Cancer Research Funds of the University of California.

We extend our thanks to Dr Robert Glaeser for discussion and criticism of the X-ray and freeze-etch models.

REFERENCES

1. ARMSTRONG, P. B., *Z. Zellforsch. Mikrosk. Anat.*, in press, (1972).
2. BRANTON, D., *Proc. Nat. Acad. Sci. USA* **55**, 1048 (1966).
3. —— *Exp. Cell Res.* **45**, 703 (1967).
4. —— *Annu. Rev. Plant. Physiol.* **20**, 209 (1969).
5. BRANTON, D. and PARK, R. B., *J. Ultrastruct. Res.* **19**, 283 (1967).
6. DEAMER, D. W., *J. Bioenergetics* **1**, 237 (1970).
7. DEAMER, D. W. and BASKIN, R. J., *J. Cell Biol.* **42**, 296 (1969).
8. DEAMER, D. W., LEONARD, R., TARDIEU, A. and BRANTON, D., *Biochim. Biophys. Acta* **219**, 47 (1970).
9. ESSNER E. S., *Protoplasma* **43**, 79 (1954).
10. GROSS, P. R., *Protoplasma* **43**, 416 (1954).
11. GURDON, J. B., *in* WILT, F. H. and WESSELLS, N. H. (Eds.), Methods in Developmental Biology p. 75. Crowell, New York, 1967.
12. HONJIN, R. and NAKAMURA, T., *J. Ultrastruct. Res.* **20**, 400 (1967).
13. HONJIN, R., NAKAMURA, T. and SHIMASAKI, S., *J. Ultrastruct. Res.* **12**, 404 (1965).
14. JAMES, R. and BRANTON, D., *Biochim. Biophys. Acta* **233**, 504 (1971).
15. JURAND, A. and SELMAN, G. G., *J. Embryol. Exp. Morphol.* **12**, 43 (1964).
16. KARASAKI, S., *J. Cell Biol.* **18**, 135 (1963).
17. —— *J. Ultrastruct. Res.* **18**, 377 (1967).
18. KARNOVSKY, M. J., *J. Cell Biol.* **27**, 137A (1965).
19. LABAW, L. W. and ROSSMANN, M. G., *J. Ultrastruct. Res.* **27**, 105 (1969).
20. LANZAVECCHIA, G., *4th Int. Conf. Electron Microsc. Berlin* Vol. 2, p. 270 (1958).
21. —— *Proc. Eur. Reg. Conf. Electron Microsc. Delft* Vol. 2, p. 746 (1960).
22. —— *J. Ultrastruct. Res.* **12**, 147 (1965).
23. MAUNSBACH, A. B., *J. Ultrastruct. Res.* **14**, 167 (1966).
24. MOOR, H. and MÜHLETHALER, K., *J. Cell Biol.* **17**, 609 (1963).
25. PETERS, A., HINDS, P. L. and VAUGHN, J. E., *J. Ultrastruct. Res.* **36**, 37 (1971).
26. REYNOLDS, E. S., *J. Cell Biol.* **17**, 208 (1963).
27. RINGLE, D. A. and GROSS, P. R., *Biol. Bull.* **122**, 263 (1962).
28. SPURR, A. R., *J. Ultrastruct. Res.* **26**, 31 (1969).
29. TERRY, R. L., *Protoplasma* **39**, 206 (1950).
30. TRELSTAD, R. L., HAY, E. D. and REVEL, J. P., *Develop. Biol.* **16**, 78 (1967).
31. WALLACE, R. A., *Biochim. Biophys. Acta* **74**, 495 (1963).
32. —— *ibid.* **74**, 505 (1963).
33. —— *ibid.* **215**, 176 (1970).
34. WALLACE, R. A. and DUMONT, J. N., *J. Cell. Physiol.*, Suppl., **72** (2), 73 (1968).
35. WARD, R. T., *J. Cell Biol.* **14**, 309 (1962).
36. WISCHNITZER, S., *Acta Embryol. Morphol. Exp.* **10**, 15 (1967).
37. WRIGGLESWORTH, J. M., PACKER, L. and BRANTON, D., *Biochim. Biophys. Acta* **205**, 125 (1970).